metals

MDPI

Article

Effect of Heat Treatment on the Microstructure and Mechanical Properties of Ti–6Al–4V Alloy Produced by L-PBF and PA-DED

Svetlana Gatina [1], Andrey Stotskiy [2], Alfiz Gareev [1], Alexander Ryzhkin [1], Irina Semenova [2,*], Alexey Mamalat [3], Olga Klimova-Korsmik [3], Sergey Zherebtsov [4] and Nariman Enikeev [1]

[1] Laboratory of Metals and Alloys Under Extreme Impacts, Ufa University of Science and Technology, 450076 Ufa, Russia; lana_gatina@mail.ru (S.G.); alfizg66@gmail.com (A.G.); alex.sandr00@bk.ru (A.R.); nariman.enikeev@gmail.com (N.E.)
[2] Laboratory of Multifunctional Materials, Ufa University of Science and Technology, 450076 Ufa, Russia; stockii_andrei@mail.ru
[3] Institute of Laser and Welding Technologies, State Marine Technical University, 198095 Saint-Petersburg, Russia; afrantende@gmail.com (A.M.); olgaklimova.ti@yandex.ru (O.K.-K.)
[4] Materials Science and Technology Department, State Marine Technical University, 198095 Saint-Petersburg, Russia; ser_z@mail.ru
* Correspondence: semenova-ip@mail.ru

Abstract

The manufacturing of personalized implants from Ti–6Al–4V alloy using additive manufacturing technologies is a promising direction in modern medicine. However, components produced by these methods are characterized by a non-equilibrium microstructure, high residual stresses, and anisotropy of mechanical properties, which necessitates subsequent heat treatment. The aim of the present work was a systematic comparative study of the effect of three heat treatment regimes—stress relief annealing (600 °C, 3 h), subtransus annealing in the (α + β) region (950 °C, 1 h, furnace cooling), and solution treatment followed by aging (STA: 950 °C, 0.5 h, water quenching + aging at 675 °C, 3 h)—on the microstructure and mechanical properties of Ti–6Al–4V alloy manufactured by laser powder bed fusion (L-PBF) and plasma arc directed energy deposition (PA-DED). The microstructure was examined using scanning electron microscopy, transmission electron microscopy, and electron backscatter diffraction (EBSD). Tensile mechanical properties were determined in two directions: parallel and perpendicular to the build direction. Stress-relief annealing led to an increase in the ductility of the alloy without a noticeable decrease in strength and without significant changes in the microstructure. Subtransus annealing resulted in the formation of an equilibrium lamellar (α + β) structure, which provided a substantial increase in ductility with a moderate decrease in strength. Solution treatment and aging resulted in formation of a bimodal microstructure. Subtransus annealing (both alloys), STA (L-PBF) and stress relief annealing (PA-DED) provided properties comparable to those of wrought material. The obtained results form the basis for a scientifically informed selection of both the manufacturing route and the heat treatment regime for biomedical implants made of Ti–6Al–4V alloy.

Keywords: Ti–6Al–4V; additive manufacturing; laser powder bed fusion; plasma arc directed energy deposition; heat treatment; microstructure; mechanical properties; biomedical implant

Check for updates

Academic Editor: Weidong Song

Received: 9 June 2026
Revised: 7 July 2026
Accepted: 11 July 2026
Published: 14 July 2026

Copyright: © 2026 by the authors. Licensee MDPI, Basel, Switzerland. This article is an open access article distributed under the terms and conditions of the Creative Commons Attribution (CC BY) license.

1. Introduction

Ti–6Al–4V alloy occupies a leading position in the production of critical medical implants (ASTM F1472, ASTM F136, ASTM F2924) due to its unique combination of high specific strength, excellent corrosion resistance in physiological environments, and biocompatibility [1]. The application of additive technologies, such as powder bed fusion (laser powder bed fusion (L-PBF) and electron beam melting (EBM)) and directed energy deposition (wire arc directed energy deposition (WA-DED)), offers great prospects for manufacturing implants for personalized medicine [2]. In particular, L-PBF allows the production of parts with anatomically accurate geometry, internal porous structures to improve osseointegration and vascular ingrowth, and controlled surface roughness, thereby contributing to shorter patient rehabilitation times [3,4]. Moreover, such porous architecture reduces the elastic modulus of the construct, thus avoiding stress-shielding effects [3,5]. Another promising method is based on WA-DED technology, which enables high-rate fabrication of large, complex-shaped parts with minimal allowance, reducing the number of machining steps and increasing the material utilization factor [6]. Among WA-DED technologies, plasma arc directed energy deposition (PA-DED) is most suitable for manufacturing medical implants because it uses a more focused and stable energy source, leading to smaller geometric deviations and improved surface quality [7]. This work is part of a complex multidisciplinary ongoing study, where biomedical tests have also been included. For example, bioactive properties of printed specimens have been successfully evaluated in [8]; however, the question of the optimal heat treatment to obtain the desired performance of printed articles under several strict and often contradictory requirements is still an open question, differently addressed by various researchers.

It is known that additive manufacturing methods produce materials with non-equilibrium microstructures, combined with specific phase transformations in the case of alloys such as Ti–6Al–4V. High cyclic melting/cooling rates and directional heat dissipation lead to the formation of columnar primary β-grains oriented along the build direction, high internal stresses and, consequently, different mechanical properties and their anisotropy as compared with traditionally treated wrought Ti alloys [9,10]. The characteristics of the as-built microstructure depend on the production method. For example, the structure obtained by L-PBF mainly consists of acicular α' martensite [11,12]. This structure provides high strength (UTS ≈ 1200–1400 MPa) but simultaneously results in low ductility ($\delta < 8\%$). The structure obtained by WA-DED methods typically consists of α-phase plates and residual β-phase. Material produced by this method exhibits lower ultimate tensile strength (900–1000 MPa) and higher ductility (7–19%) [13,14]. The differences in the micro- and macrostructure of the Ti–6Al–4V alloy produced by L-PBF and WA-DED are related to different heat inputs and different melt pool volumes and cooling rates (10–600 K/s for WA-DED, 10^4–10^8 K/s for L-PBF) [13,15–18].

Thus, additively manufactured material by combination of strength and ductility is inferior to the Ti–6Al–4V alloy processed by conventional thermomechanical treatment. Strategies aimed at improving the structural homogeneity and mechanical characteristics of additively manufactured Ti–6Al–4V include modifying the chemical composition by microalloying, as well as interlayer forging, which promotes grain refinement and reduces anisotropy [19–21]. During fabrication, a significant effect can be achieved by optimizing parameters, including scanning speed, feed rate, and overall heat input [22,23]. However, many of these approaches are either limited in terms of their application to finished complex-shaped parts or involve significant time and resource costs. The simplest, most flexible, and most cost-effective method for the final tailoring of microstructure and properties, applicable also to personalized biomedical implants, is heat treatment (HT). The applied HT regimes must ensure stress relief and achieve the required ductility

($\delta \geq 10\%$, ASTM F2924, ASTM F1472) while maintaining high ultimate tensile strength (UTS $\geq$ 895 MPa), and consequently high fatigue strength. It is known that the phase composition and morphology of structural elements significantly affect the mechanical characteristics of the alloy [16,24]. Regarding the effect on the structural-phase state, several main types of HT applied to additively manufactured Ti–6Al–4V are distinguished: (i) stress-relief annealing at 600–750 °C for 1–4 h; (ii) subtransus annealing at 800–950 °C for 1–2 h with slow furnace cooling to obtain a coarse-lamellar equilibrium ($\alpha + \beta$) structure; (iii) solution treatment from 900–950 °C followed by aging at 480–750 °C for 2–8 h (STA) to form a bimodal ($\alpha + \beta$) structure [25–27].

Thus, the question of developing a reasonable strategy for the final treatment of 3D-printed finished articles is still a matter of discussion, one that also assumes a variety of printing techniques which produce markedly different structural and phase states. We present the results of in-depth studies on specimens of materials that share the same chemical composition and which have been 3D-printed by two different additive manufacturing techniques: powder-bed (L-PBF) and wire-based (PA-DED). These studies have been carried out in a systematic and consistent way, with several complimentary techniques showing striking differences in microstructure and mechanical behavior among the workpieces produced by these two techniques and by similar heat treatments, while also discussing the underlying issues.

We demonstrate that standard heat treatment for residual stresses release is far from optimal, as it provides a rather undesired combination of mechanical properties. Moreover, based on previous research [28], we show that the treatments which provide the combination of properties outperforming the performance of conventionally treated Ti64 alloy could also have little practical meaning since such procedures as multi-cycle heat treatment can hardly be reproduced within a robust post-additive manufacturing treatment feasible in mass production, in particular, medical implants. Therefore, we propose possible compromises based not only on mechanical performance but also on applicability in industrial conditions. Accordingly, the aim of this work is to experimentally justify the choice of heat treatment regime for a Ti–6Al–4V alloy produced by L-PBF and PA-DED that provides the best combination of strength, ductility, and isotropy of properties, satisfying the requirements for biomedical implants.

2. Materials and Methods

The study was performed on Ti–6Al–4V alloy specimens produced by L-PBF and PA-DED.

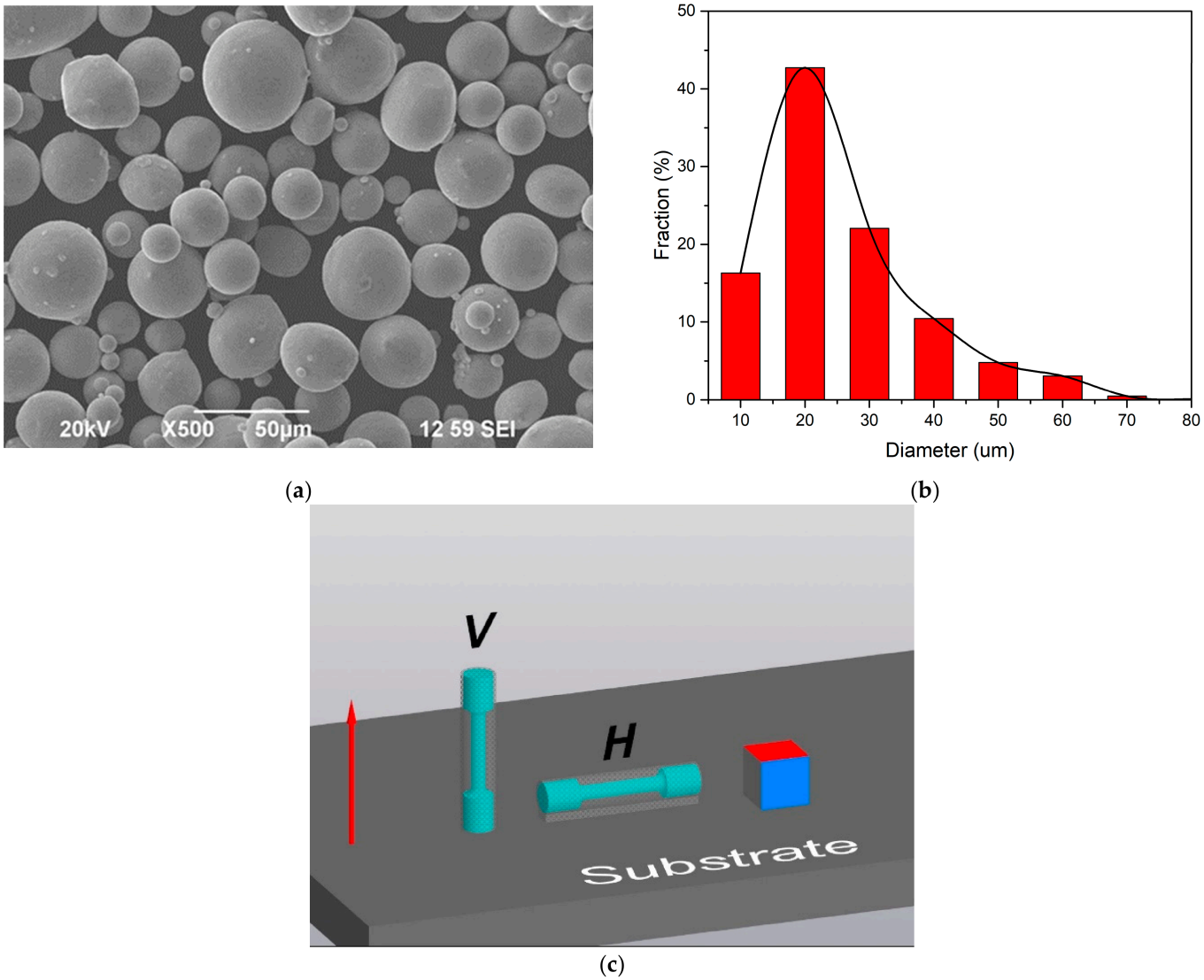
2.1. L-PBF

L-PBF was carried out using a BLT-A160 printer (Bright Laser Technologies Co., Xi'an, China) under an Ar atmosphere. The laser wavelength was 1060–1080 nm, and the beam diameter was 40 μm. The detailed printing parameters are described in [28].

Ti–6Al–4V powder manufactured by the plasma atomization method in an Ar atmosphere was used (NORMIN Ltd., Borovichi, Russia). The chemical composition of the powder, determined by energy-dispersive X-ray spectroscopy (EDS) (AZtecLive Lite Xplore 30, Oxford Instruments, Abingdon, UK), is given in Table 1. The average powder particle size was 25 ± 5 μm (Figure 1a). A histogram of particle size distribution is shown in Figure 1b. The β-transus temperature was determined by differential scanning calorimetry using a simultaneous thermal analyzer (Netzsch 409 PC/4/H, Netzsch-Gerätebau GmbH, Selb, Germany) and subsequently confirmed by trial quenching. It was found to be 982 ± 5 °C.

Table 1. Chemical composition of Ti–6Al–4V powder (wt%).

Ti	Al	V	Fe	Other
90.5 ± 0.3	5.7 ± 0.2	3.6 ± 0.3	0.2 ± 0.1	<0.1



(**a**) (**b**)

(**c**)

Figure 1. Laser powder bed fusion (L-PBF) Ti–6Al–4V: (**a**) scanning electron microscopy (SEM) image of the powder; (**b**) histogram showing the powder particle size distribution; (**c**) appearance of the as-built specimens, the red arrow indicates the building direction.

For tensile testing, cylindrical blanks 7 mm in diameter and 32 mm in length were printed in the horizontal (H) and vertical (V) directions. For microstructural examination, cubes with an edge length of 10 mm were printed (Figure 1c).

2.2. PA-DED

Wire deposition was performed using a plasma torch for layer-by-layer welding, developed at Perm National Research Polytechnic University (Perm, Russia). A drawn wire with a diameter of 1.6 mm was used. The detailed deposition parameters are given in [29]. The chemical composition of the wire, determined by EDS, is shown in Table 2. The β-transus temperature was found to be 989 ± 5 °C.

Table 2. Chemical composition of Ti–6Al–4V wire (wt%).

Ti	Al	V	Fe	Other
90.2 ± 0.2	5.8 ± 0.1	4.0 ± 0.2	0.2 ± 0.1	<0.1

A wall with a height of 50 mm, a length of 180 mm and a width of 10 mm was produced. From this wall, blanks for tensile tests (cylinders 7 mm in diameter, 32 mm in length) were cut in the build direction (V) and perpendicular to the build direction (H). Specimens for microstructural studies were cut as cubes with an edge of 10 mm. All specimens for microstructure analysis and for H-direction tensile testing were taken from the middle of the wall's height (Figure 2).

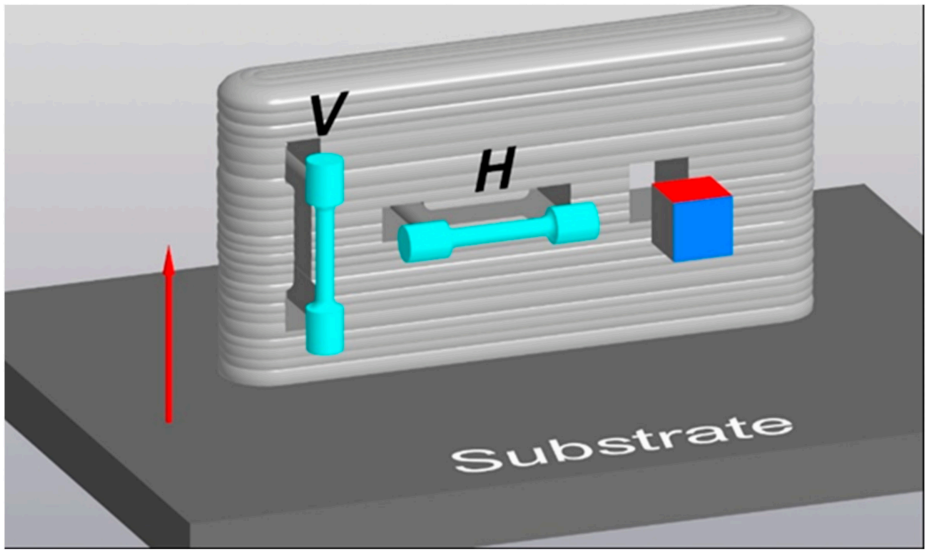


Figure 2. Scheme of specimen cutting from the plasma arc directed energy deposition (PA-DED) wall. The red arrow indicates the building direction.

It is noteworthy that the variation in the content of the principal alloying elements (Al, V) and impurity elements in the specimens produced by L-PBF and PA-DED, relative to the initial materials (powder and wire, respectively), falls within the detection limit of the EDS method (~0.1–0.2 wt.%). These observations are in agreement with the results of our previous study [8].

2.3. Heat Treatment

Three types of heat treatment (HT) were performed in a muffle furnace (Nabertherm GmbH, Lilienthal, Germany). Stress-relief annealing was carried out at 600 °C for 3 h with furnace cooling (FC). Subtransus (α + β) annealing was conducted at 950 °C for 1 h with FC. Both stress-relief and subtransus annealing were performed under an Ar atmosphere. Solution treatment and aging (STA): samples were heated to 950 °C in air, held for 30 min, then water quenched (WQ) and subsequently aged at 675 °C for 3 h, followed by air cooling (AC). The solution treatment was performed in air because the furnace door had to be opened for immediate water quenching, which would compromise an inert atmosphere.

2.4. Microstructural Investigation

The macrostructure of as-built samples was examined using a optical microscope (4XS, Vostok-7, Moscow, Russia). Microstructure investigations were performed using a Tescan Mira 3 field-emission scanning electron microscope (SEM) (Tescan, Brno, Czech Republic) equipped with an Oxford C-NANO+ electron backscatter diffraction (EBSD) system

(Oxford Instruments, Abingdon, UK). Up to 11 Kikuchi bands were used for pattern indexing to reduce indexing errors. EBSD data were analyzed with AZtec Crystal software 2.1. Standard EBSD acquisition was applied with a tilt angle of 70°, an accelerating voltage of 20 kV and a beam current of 20 nA. For all conditions, maps of 188 × 188 μm^2 were recorded with a step size of 0.35 μm. Final surface preparation was performed with an AL-2200 ion-beam milling and polishing machine (Beijing Ion Beam Technology Co., Beijing, China) using 99.99% argon gas. The polishing regime was 3 kV, 0.4 mA for 2 h.

Fine-structure investigations were performed with a Jeol 2100 transmission electron microscope (TEM) (Jeol, Tokyo, Japan) operated at 200 kV. TEM foils were prepared by electropolishing in a Tenupol-5 Struers device (Struers, Ballerup, Denmark) using an electrolyte of 60% methanol, 35% butanol and 5% perchloric acid.

All specimens for structural studies were cut at a depth of 2 mm from the surface to avoid the influence of an α-enriched surface layer.

2.5. Mechanical Testing

Tensile testing was conducted at room temperature (20 °C) using an Instron 5982 machine (Instron, Norwood, MA, USA) at a strain rate of 10^{-3} s^{-1}. The force measurement accuracy was 1%. Cylindrical blanks in the as-built and heat-treated conditions were machined to remove the oxide layer and to produce standard dog-bone tensile specimens with a gauge diameter of 3 mm and gauge length 15 mm. The tests were conducted in accordance with ISO 6892-1:2019 [30]. Three samples were tested for each studied condition.

3. Results

3.1. As-Built Microstructure

Figure 3 shows macrostructure images of a Ti–6Al–4V alloy produced by L-PBF and PA-DED. In the cross-section perpendicular to the build direction, the grains are equiaxed (Figure 3a,c). Along the build direction, columnar grains are observed (Figure 3b,d). The grain size differs significantly between the two methods. In the cross-section of L-PBF samples, the average grain size is 94 ± 12 μm, and their length ranges from 60 to 630 μm. In the PA-DED alloy, the grains are much larger: the cross-sectional size is 1300 ± 100 μm, and the average grain length reaches 3000 ± 500 μm. Figure 3d clearly shows grains growing through several layers.

For detailed microstructural examination EBSD and SEM in backscattered electron (BSE) regime were used. Figure 4a presents an EBSD map of the L-PBF alloy. A complex hierarchical acicular structure is observed. Large needles form packets. The length of the primary large needles ranges from 7 to 35 μm, and the width from 0.3 to 3 μm. According to TEM images, the average length of the secondary fine needles is 1.0 ± 0.2 μm, and the width is 0.25 ± 0.05 μm (Figure 5a). Inside the primary needles, dislocation tangles and twins are also found (Figure 5b). Phase maps indicate that 99.9% of the structure has an HCP lattice, corresponding to α/α′ phases. The uniform contrast in the BSE image of the structure (Figure 4b) also confirms the absence of β-phase.

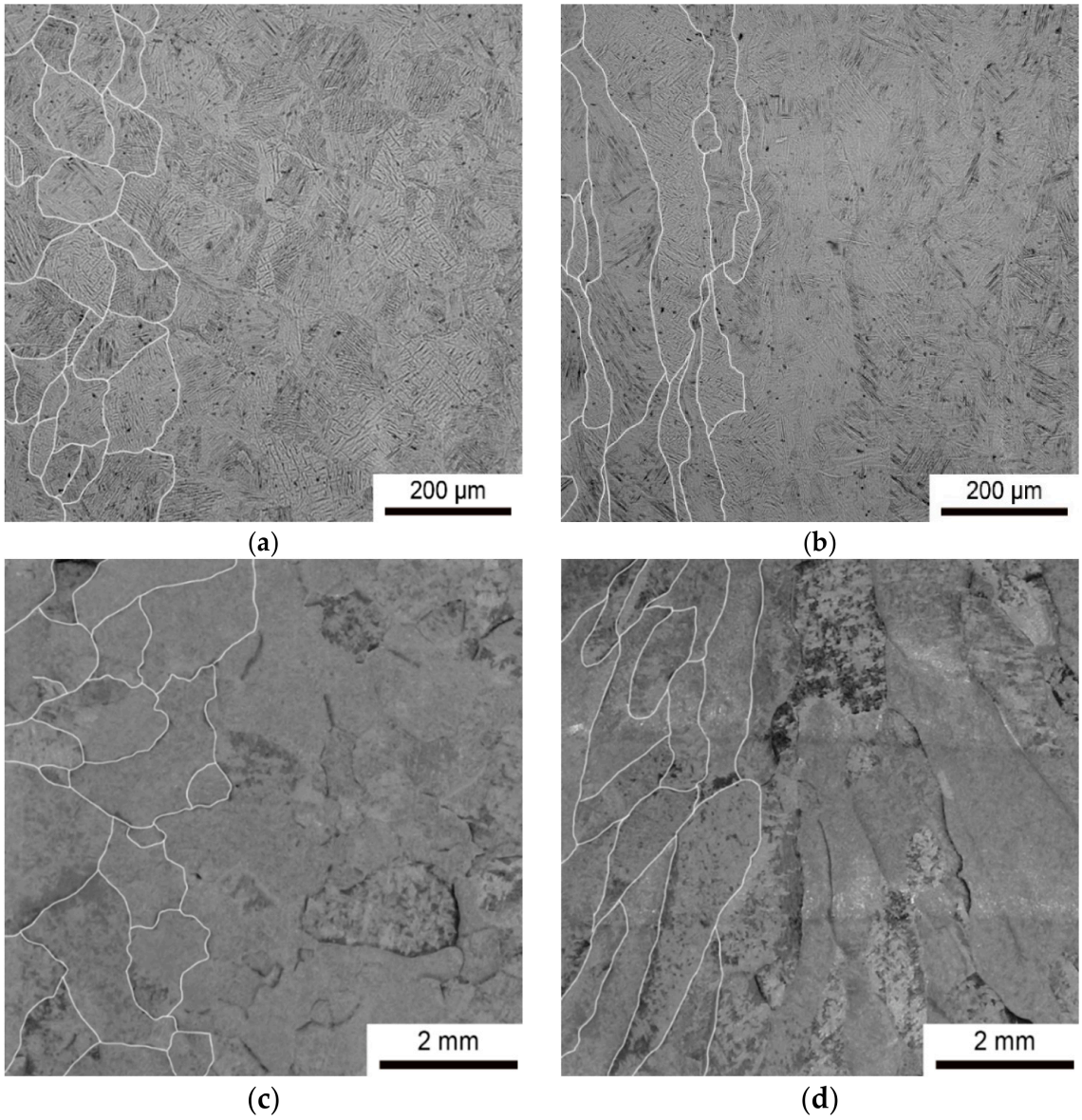


Figure 3. Macrostructure of Ti–6Al–4V alloy produced by (**a**,**b**) L-PBF; (**c**,**d**) PA-DED; (**a**,**c**) cross-section; (**b**,**d**) longitudinal section.

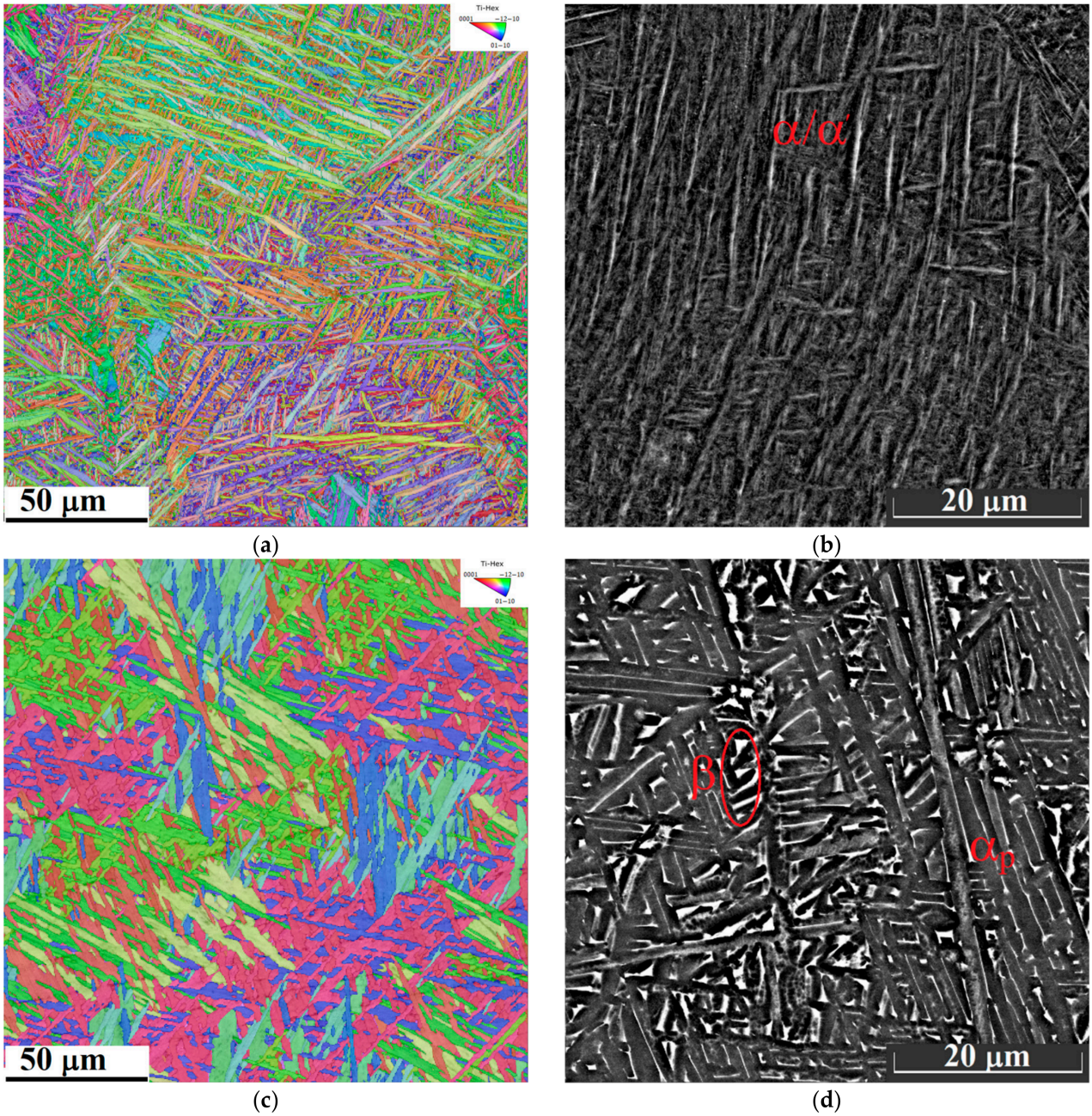


Figure 4. Microstructure of Ti–6Al–4V alloy produced by (**a**,**b**) L-PBF; (**c**,**d**) PA-DED; (**a**,**c**) electron backscatter diffraction (EBSD); (**b**,**d**) backscattered electron (BSE).

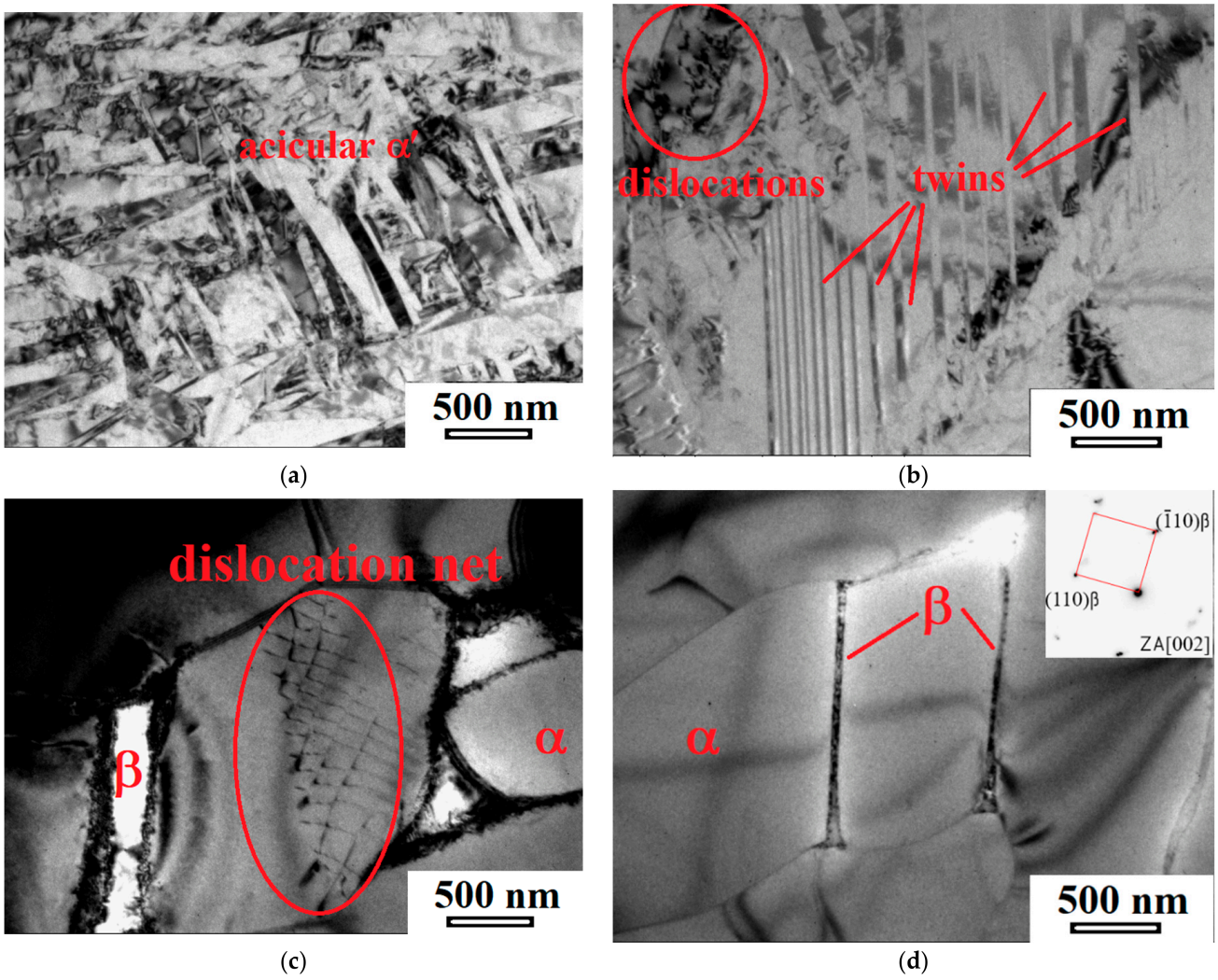


Figure 5. TEM images of the microstructure of Ti–6Al–4V alloy produced by: (**a**,**b**) L-PBF; (**c**,**d**) PA-DED.

The EBSD map of the PA-DED sample shows a basket-weave microstructure consisting of plates with an HCP lattice (Figure 4c). Non-uniform contrast in BSE images indicates the presence of two phases. Bright regions correspond to the β-phase, dark regions to α (Figure 4d). The width of α-plates varies from 1 to 6 μm, and the length ranges from 5 to 40 μm. The β-phase, with a volume fraction of 9 ± 0.5%, is observed as interlayers between α-plates. TEM images show dislocation tangles and nets in some α-grains, but the majority of the structure is dislocation free (Figure 5c,d). Overall, the PA-DED structure has a lower defect density compared with the L-PBF alloy.

3.2. Effect of Heat Treatment on the Microstructure

3.2.1. Stress-Relief Annealing

Stress-relief annealing did not cause noticeable microstructural changes (Figure 6).

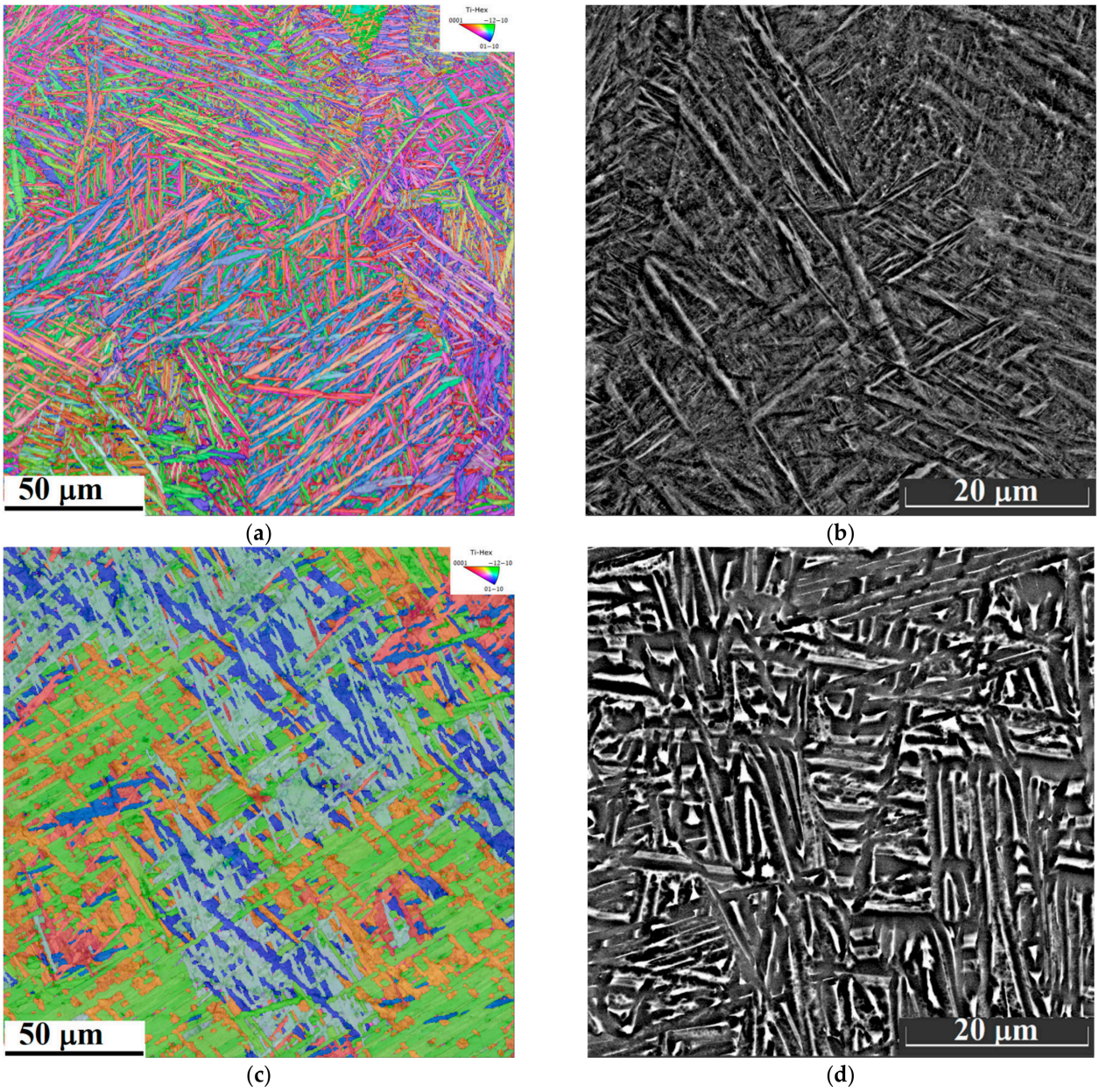


Figure 6. Microstructure of Ti–6Al–4V alloy after stress-relief annealing, produced by (**a**,**b**) L-PBF; (**c**,**d**) PA-DED; (**a**,**c**) EBSD; (**b**,**d**) BSE.

3.2.2. Subtransus Annealing

After subtransus annealing, a two-phase (α + β) coarse-lamellar structure formed (Figure 7). In the L-PBF alloy, the length of α-plates ranges from 7 to 42 μm, and the width from 0.5 to 7 μm. The formation of equiaxed α-particles with a diameter of 5 ± 0.5 μm (volume fraction 24%) is observed (Figure 7a). The β-phase (BCC lattice) precipitated as interlayers between α-plates; its volume fraction was 7.4 ± 0.2% (Figure 7b). In the PA-DED alloy, a similar structure formed (Figure 7c). The α-plates widened compared with the as-built state, and the β-phase volume fraction remained within the error range at 8.4 ± 1% (Figure 7d).

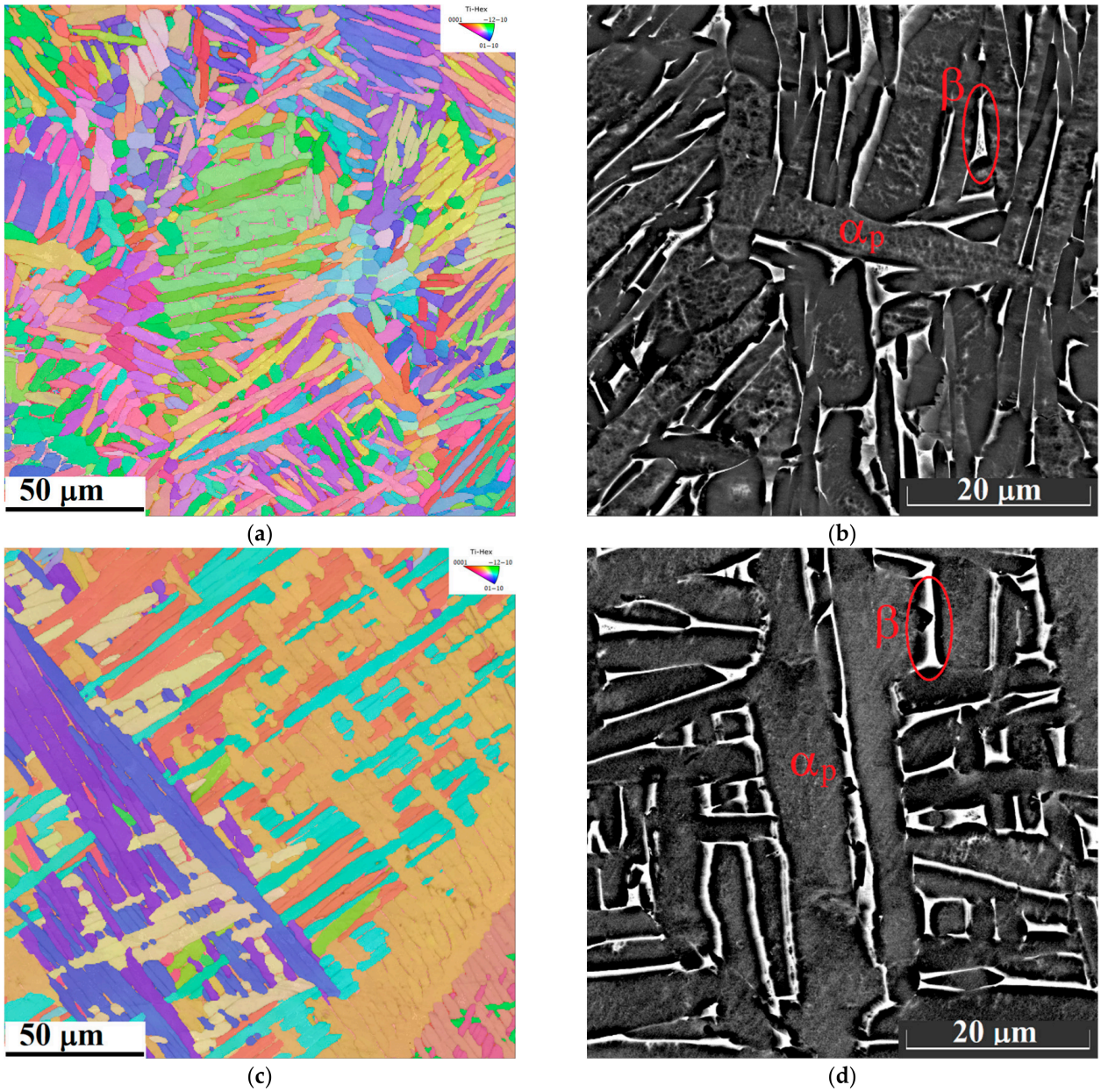


Figure 7. Microstructure of Ti–6Al–4V alloy after subtransus annealing, produced by (**a**,**b**) L-PBF; (**c**,**d**) PA-DED; (**a**,**c**) EBSD; (**b**,**d**) BSE.

3.2.3. Solution Treatment and Aging

STA leads to the formation of a bimodal structure consisting of coarse plates and globules of primary α-phase and a fine mixture of secondary α and β-phases (Figure 8). The volume fraction of β-phase was 6.4 ± 1.2% in L-PBF samples and 7.7 ± 0.9% in PA-DED samples.

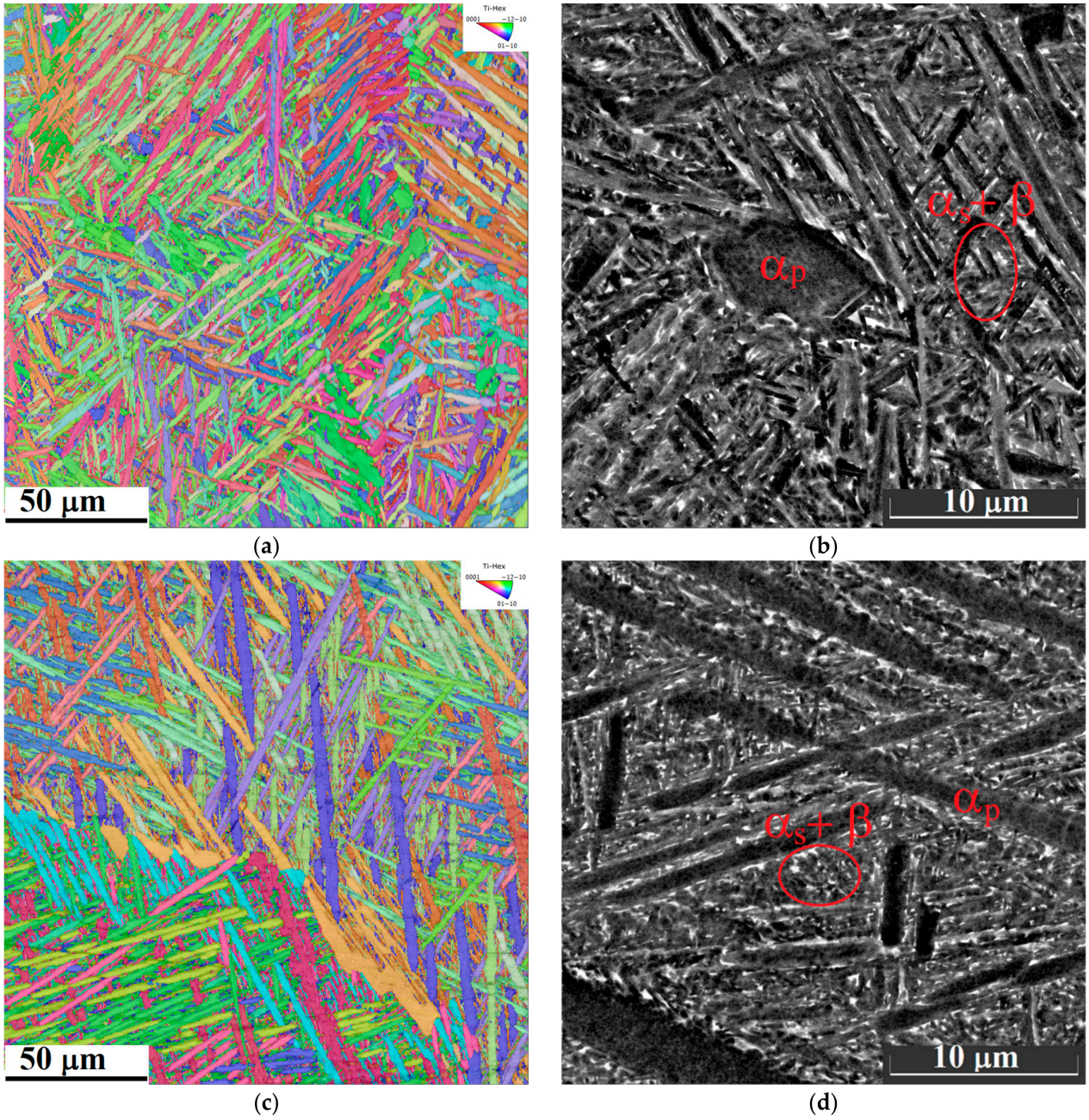
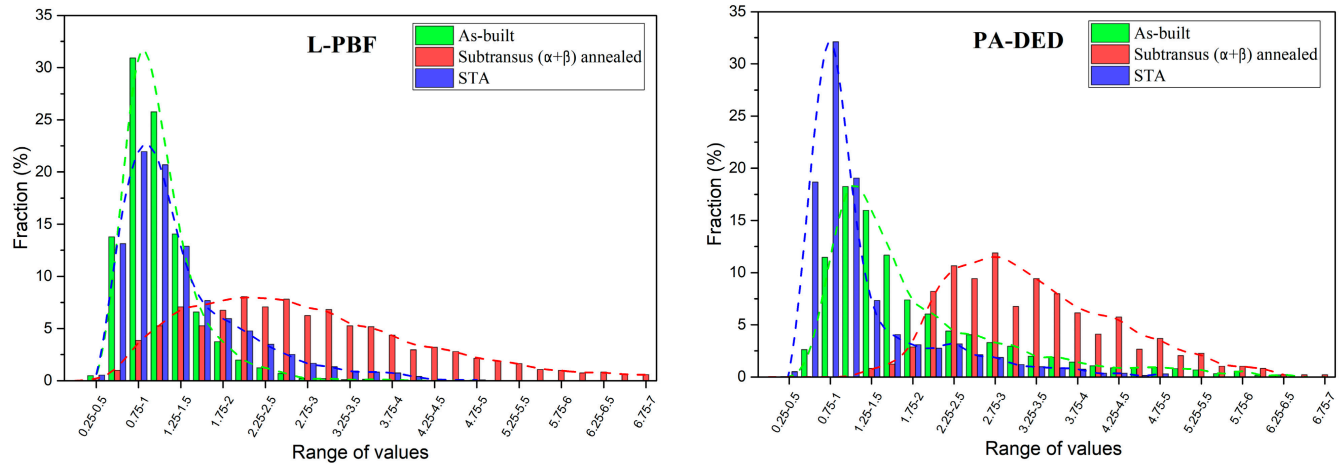


Figure 8. Microstructure of the Ti–6Al–4V alloy after solution treatment and aging (STA), produced by (**a**,**b**) L-PBF; (**c**,**d**) PA-DED; (**a**,**c**) EBSD; (**b**,**d**) BSE.

Figure 9 shows the dependence of α/α'-plate width on the heat treatment regime. Subtransus annealing leads to significant plate widening compared with the as-built state. The size distribution peak becomes less sharp, indicating the formation of a more homogeneous structure. However, STA has a different effect on the structural parameters of L-PBF and PA-DED alloys. In the L-PBF alloy, plates widen (the peak shifts towards larger values). In contrast, in the PA-DED alloy, STA increases the fraction of narrow plates.

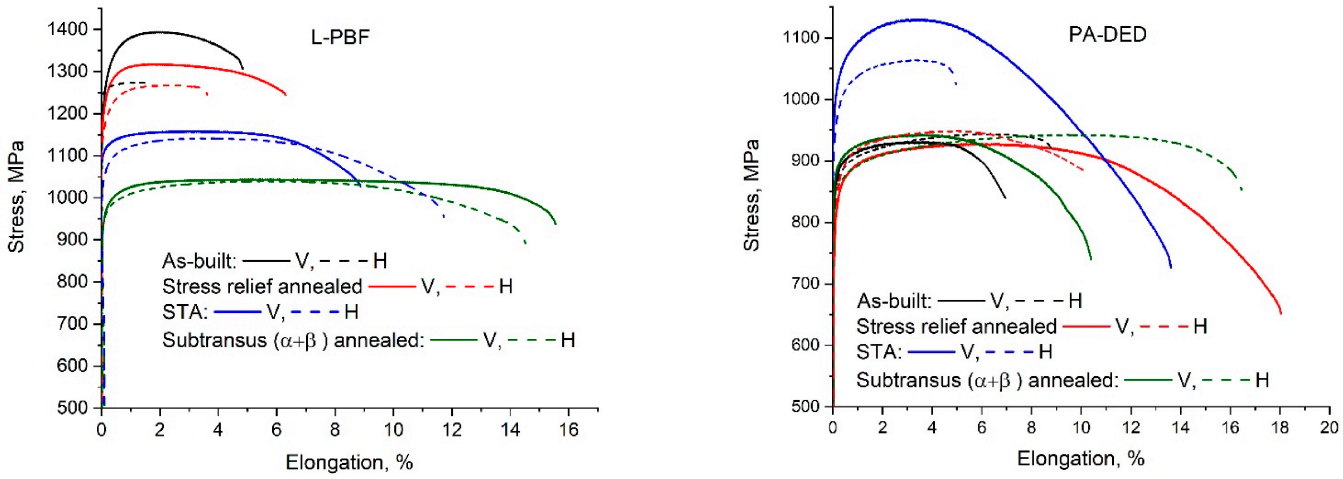


(**a**) (**b**)

Figure 9. Effect of heat treatment on the width of α/α′-plates in the alloy produced by (**a**) L-PBF; (**b**) PA-DED.

3.3. Mechanical Properties

Figure 10 presents the tensile test results. Vertical L-PBF samples exhibit the highest strength but low ductility (Figure 10a). Horizontal samples are significantly inferior in mechanical properties to vertical ones (Table 3). Stress-relief annealing increases both uniform and total elongation with a slight decrease in strength; however, elongation to failure does not exceed 7%. STA, along with increased ductility, reduces strength. The highest values of uniform and total elongation are observed after subtransus annealing, though these samples have the lowest strength.



(**a**) (**b**)

Figure 10. Mechanical properties of the Ti–6Al–4V alloy produced by (**a**) L-PBF; (**b**) PA-DED.

Table 3. Mechanical properties of Ti–6Al–4V alloy produced by L-PBF and PA-DED compared with wrought alloy.

	Treatment	UTS, MPa		YS, MPa		uEL, %		EL, %	
		V	H	V	H	V	H	V	H
L-PBF [this study]	As-built	1395 ± 10	1275 ± 12	1282 ± 10	1111 ± 15	2 ± 0.2	2 ± 0.2	4.8 ± 1.2	3.3 ± 0.5
	Stress relief annealing	1317 ± 7	1273 ± 5	1253 ± 7	1190 ± 8	2.2 ± 0.2	2.5 ± 0.2	6.3 ± 1	3.7 ± 0.5
	Subtransus annealing	1042 ± 5	1042 ± 5	985 ± 12	970 ± 6	7 ± 0.1	8.1 ± 0.6	15.6 ± 1	14.4 ± 1
	STA	1157 ± 12	1141 ± 10	1127 ± 10	1075 ± 5	4.2 ± 0.1	3.9 ± 0.2	8.9 ± 0.5	11.5 ± 0.6
PA-DED [this study]	As-built	930 ± 7	942 ± 3	882 ± 10	874 ± 4	3.6 ± 0.5	7.2 ± 0.5	6.7 ± 1.5	8.9 ± 2.3
	Stress relief annealing	927 ± 10	948 ± 5	834 ± 7	850 ± 8	7.7 ± 1.5	5.2 ± 0.5	18 ± 4	10 ± 2
	Subtransus annealing	941 ± 5	942 ± 6	890 ± 8	860 ± 10	4 ± 0.1	10.6 ± 1.2	10.4 ± 2	16.5 ± 3
	STA	1130 ± 10	1064 ± 5	1027 ± 5	980 ± 6	3.6 ± 0.1	3.5 ± 0.1	13.6 ± 2	5 ± 1.5
L-PBF	As-built [26,31,32]	1133–1200		986–1022		-		3.4–11	
	Stress relief annealing [26,31,32]	980–1115		1045–1054		-		10–12	
	Subtransus annealing [26,31]	950–988		905–911		-		9.5–16	
	STA [32]	781 ± 8		-		-		3.6 ± 0.6	
WA-DED	As-built [18,27]	820–847		710–746		-		7.2–12.2	
	Stress relief annealing [18,27]	872–854		766–772		-		10.9–11.8	
	Subtransus annealing [18]	810 ± 9.04		721 ± 16.4		-		11.5 ± 4.15	
	STA [18,27]	918–1034		858–931		-		5.9–7.5	
Wrought	As-received [33]	1016–1074		965–1021		-		15	
	Subtransus annealing [34]	926 ± 2		878 ± 4		-		20 ± 1	
	STA [33,35,36]	1028–1120		925–1050		-		10–16.3	

PA-DED samples have lower strength than L-PBF samples. Stress-relief and subtransus annealing increase ductility while maintaining strength. STA significantly enhances strength but drastically reduces the ductility of horizontal samples (Figure 10b).

4. Discussion

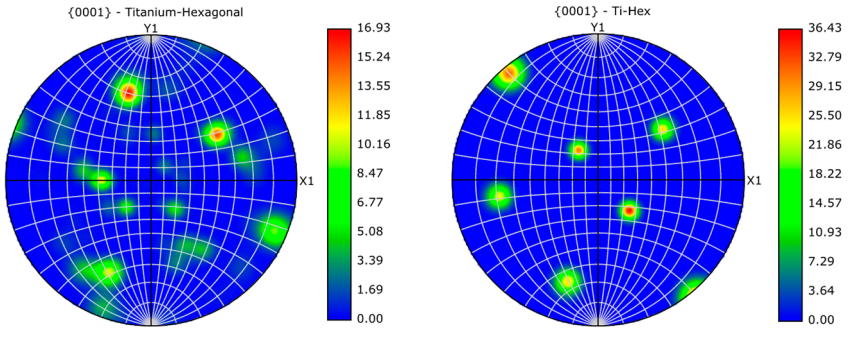
This work investigates the effect of heat treatment on the microstructure and mechanical properties of Ti–6Al–4V alloy produced by two different additive manufacturing methods, L-PBF and PA-DED, both of which are promising for bio-implant applications. The study was carried out in two directions: vertical (build direction) and horizontal (perpendicular to the build direction).

The experimental data confirm that the as-built microstructure of the alloy produced by both methods consists of columnar primary β-grains oriented along the build direction. However, there are distinctive features in the macro- and microstructure. The size

of primary β-grains in the PA-DED alloy reaches several millimeters, which is tens of times larger than that in the L-PBF alloy. According to EBSD analysis, the L-PBF alloy exhibits a hierarchical acicular α/α′ structure with an HCP lattice; the fraction of the BCC β-phase is 0.1%. As the α and α′ phases have the same lattice with similar parameters, it is difficult to distinguish each of them by X-ray diffraction or EBSD. Nevertheless, it is reported [12,31,37] that, due to the high cooling rate (>10^4 K/s), the L-PBF alloy is completely martensitic. Furthermore, the absence of grain-boundary α-phase in the IPF EBSD maps (Figure 4a) also indicates a complete martensitic β → α′ transformation [31,38]. Martensite enriched with the β-stabilizer V provides strong solid-solution strengthening [31]. High melt solidification rates produce a high density of dislocations and twins [28,39]. This non-equilibrium ultrafine structure gives the alloy high strength (1395 MPa and 1275 MPa in the vertical and horizontal sections, respectively) but very low ductility (4.8% and 3.3%).

The microstructure of the PA-DED alloy consists of HCP plates forming a basket-weave pattern. The high fraction (9%) of the β-phase is associated with the slower cooling rate of the melt. Such a Widmanstätten (α + β) structure is typical for these additive manufacturing methods [10]. The strength of the PA-DED samples is considerably lower than that of the L-PBF material, while the ductility is almost twice as high (UTS: 930 MPa (V), 942 MPa (H); EL: 6.7% (V), 8.7% (H)). This is attributed to the formation of a more equilibrium and coarse-grained structure.

The L-PBF samples exhibit much stronger strength anisotropy than the PA-DED samples. This is due to the different phase transformation mechanisms upon cooling. During the β → α/α′ transformation, the new phase (α or α′) precipitates within the primary β-grains strictly according to the Burgers orientation relationship [39]. Theoretically, up to 12 crystallographically distinct α′ variants can form from a single β-grain. However, in L-PBF, because of the extremely high cooling rate and steep thermal gradient, variant selection occurs and only a few of the 12 possible variants are realized [26,40,41]. In our case, primary α′ laths with the same orientation grow through the β-grain parallel to each other. Between the primary laths, fine secondary α′ laths form, which are also parallel to each other but are not parallel to the primary laths. This parallel mechanism, which differs from classical self-accommodation (triple clusters), leads to a sharp texture and, consequently, to pronounced anisotropy of mechanical properties. At the same time, during the PA-DED method, each previous layer is subjected to multiple cyclic heating, which leads to partial dissolution of the formed α-phase and the emergence of new crystallographic variants. Variant selection weakens, the texture becomes more random, and property anisotropy decreases [40,41]. Thus, the PA-DED pole figure exhibits a greater number of basal plane misorientations compared with the L-PBF sample (Figure 11).



(**a**) (**b**)

Figure 11. The pole figures of the Ti–6Al–4V alloy produced by (**a**) L-PBF; (**b**) PA-DED.

After stress-relief annealing at 600 °C, strength is maintained and ductility increases, which is likely due to a reduction in internal stresses. However, no noticeable microstructural changes occur. It has been established [42,43] that temperatures below 700–800 °C cause only partial decomposition of martensite in L-PBF material. In [18], it was demonstrated that stress relief annealing improved the ductility by over 30% while not coarsening the grain size in WA-DED material.

Subtransus annealing leads to the formation of a two-phase (α + β) lamellar structure. In the PA-DED alloy, the α-plates are coarser because of the larger initial size of the primary β-grains. This annealing reduces strength and increases ductility in both alloys compared with the as-built state, owing to the relief of internal stresses, a transition to a more equilibrium condition, coarsening of structural elements, and the formation of a sufficient amount of β-phase (≈7–8%), which has a BCC lattice with more slip systems than the HCP lattice of the α-phase. The L-PBF alloy retains higher strength than PA-DED, which agrees well with the Hall–Petch relationship. After this heat treatment, both alloys become nearly isotropic in strength. A similar effect of subtransus annealing on mechanical properties has been reported in numerous studies on additively manufactured Ti–6Al–4V [18,26,31].

STA has a different effect on the structure and mechanical properties. In L-PBF samples, the structure coarsens due to martensite decomposition and the precipitation of (α + β)-phases. The transition to the stable (α + β)-state reduces strength and increases ductility. A softening effect of STA in L-PBF material has also been reported in [32]. In PA-DED samples, ageing conversely leads to a reduction in the average α-plate size. This is explained by partial dissolution of primary α_p-plates upon heating to 950 °C and the formation of a fine secondary α_s-phase during subsequent ageing. In this case, STA acts as a strengthening heat treatment for the PA-DED alloy, similar to wrought material [36]. Similarly, in [18] STA increased strength by 12% and reduced ductility by 30%. However, these samples exhibit strongly anisotropic properties. It is likely that upon solution treatment, the intragranular α-phase dissolves first, while the grain-boundary α_{GB}-phase is retained as a layer (Figure 12) [43]. During subsequent tensile testing, the grain-boundary α-phase acts as a stress concentrator; strain localizes at the α/β interphase boundaries. In horizontal samples, crack propagation and failure occur along the boundaries of columnar β-grains. Consequently, horizontal samples are significantly inferior in strength and ductility to vertical samples, where the crack path is more tortuous. In PA-DED samples after subtransus annealing, which have a more homogeneous Widmanstätten structure, strain distribution is uniform, and thus the deleterious effect of the grain-boundary α-phase observed in the STA condition is not seen.

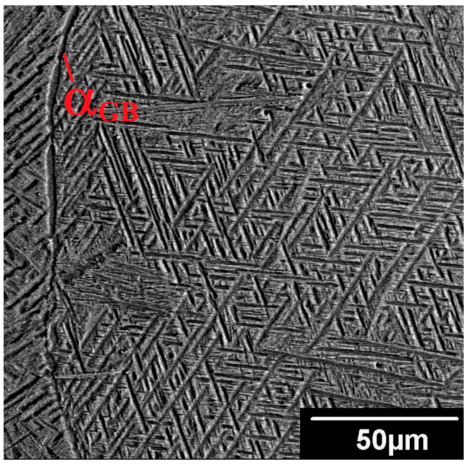


Figure 12. Grain boundary α_{GB}-phase in Ti–6Al–4V alloy produced by PA-DED after STA.

Furthermore, a large statistical scatter in ductility is observed in PA-DED samples. This scatter is likely associated with the coarse primary β grains, whose size (several millimeters) is comparable to the gauge diameter (3 mm) of the standard tensile specimens. Studies [10,44] have demonstrated that a limited number of grains within the gauge volume leads to significant variability in measured properties. To address this limitation in future work, specimens with a larger cross-section should be used for mechanical testing of PA-DED and other WA-DED materials.

In the L-PBF alloy, the mechanical properties after subtransus annealing and STA satisfy the requirements of ASTM F2924 (UTS $\geq$ 895 MPa, YS $\geq$ 825 MPa, EL $\geq$ 10%). In the PA-DED alloy, the requirements of ASTM F2924 are met after stress-relief and subtransus annealing.

Thus, properly selected heat treatment allows additively manufactured Ti–6Al–4V alloy to achieve mechanical properties comparable to or even exceeding those of wrought material (Table 3), opening up broad possibilities for personalized implantology. However, it should be noted that the present study is limited to microstructural analysis and tensile testing. No fatigue, corrosion, or biocompatibility data are presented, which are also critical for biomedical applications. Therefore, the final recommendations for specific implant applications should be considered preliminary. For example, for parts requiring a balance of strength, high ductility and isotropy (load-bearing implants), L-PBF followed by subtransus annealing appears reasonable. Maximum strength can be achieved with STA, but at the cost of isotropy. For large implants with moderate loads (cranial plates, long bones), PA-DED combined with subtransus or stress-relief annealing is recommended.

5. Conclusions

The obtained results demonstrate that appropriate heat treatment can yield mechanical properties comparable to those of wrought Ti–6Al–4V alloy. However, the suitability of these materials for biomedical implants requires further validation through fatigue, corrosion, and biocompatibility testing. The specific findings of this study are as follows.

As a result of the performed investigations, it has been established that the additive manufacturing method strongly affects the initial microstructure and mechanical properties of the Ti–6Al–4V alloy and, consequently, the subsequent response to heat treatment.

1. It was established that L-PBF forms a non-equilibrium martensitic structure with a high defect density in the alloy, which provides high strength at low ductility. In contrast, PA-DED forms an equilibrium Widmanstätten (α + β) structure, which exhibits moderate strength and high ductility.
2. It was shown that stress-relief annealing does not lead to noticeable microstructural changes; an increase in ductility is observed while strength is preserved.
3. It was revealed that subtransus annealing forms an equilibrium lamellar (α + β) structure, after which both alloys become nearly isotropic in strength and their ductility increases substantially.
4. It was established that solution treatment and aging (STA) form a bimodal structure, but its effect is fundamentally different: for L-PBF it provides high strength with adequate ductility, whereas for PA-DED it drastically increases strength but severely reduces the ductility of horizontal samples.

Author Contributions: Conceptualization, N.E., S.Z. and I.S.; methodology, A.R., O.K.-K. and A.S.; validation, S.G., A.S. and O.K.-K.; formal analysis, S.G., A.S. and A.M.; investigation, S.G., A.G., A.S., A.R. and A.M.; resources, N.E. and O.K.-K.; data curation, A.S., A.M., A.R. and A.G.; writing—original draft preparation, S.G.; writing—review and editing, I.S., S.Z. and N.E.; visualization, A.S.,

A.G. and A.M.; supervision, N.E.; project administration, S.Z. and I.S.; funding acquisition, N.E. All authors have read and agreed to the published version of the manuscript.

Funding: This research was funded by the Russian Science Foundation grant No. 23-69-10003.

Data Availability Statement: The original contributions presented in this study are included in the article material. Further inquiries can be directed to the corresponding author.

Acknowledgments: Experimental studies were performed using the equipment of the "Nanotech" Resource Sharing Center of Ufa University of Science and Technology.

Conflicts of Interest: The authors declare no conflicts of interest.

Abbreviations

The following abbreviations are used in this manuscript:

AC	Air cooling
BCC	Body centered cubic
BSEs	Backscattered electrons
EBM	Electron beam melting
EBSD	Electron backscatter diffraction
EDS	Energy dispersive X-ray spectroscopy
EL	Elongation
FC	Furnace cooling
HCP	Hexagonal close packed
HT	Heat treatment
L-PBF	Laser powder bed fusion
PA-DED	Plasma arc directed energy deposition
PBF	Powder bed fusion
SEM	Scanning electron microscopy
STA	Solution treatment and aging
TEM	Transmission electron microscopy
uEL	Uniform elongation
UTS	Ultimate tensile strength
WA-DED	Wire arc directed energy deposition
WQ	Water quenching
YS	Yield strength

References

1. Kaur, M.; Singh, K. Review on Titanium and Titanium Based Alloys as Biomaterials for Orthopaedic Applications. *Mater. Sci. Eng. C* **2019**, *102*, 844–862. [CrossRef] [PubMed]
2. Gao, Y.; Jiang, W.; Zeng, D.; Liang, X.; Ma, C.; Xiao, W. Additive Manufacturing of Titanium Alloys for Biomedical Applications: A Systematic Review. *Rev. Mater. Res.* **2025**, *1*, 100011. [CrossRef]
3. Kiselevskiy, M.V.; Anisimova, N.Y.; Kapustin, A.V.; Ryzhkin, A.A.; Kuznetsova, D.N.; Polyakova, V.V.; Enikeev, N.A. Development of Bioactive Scaffolds for Orthopedic Applications by Designing Additively Manufactured Titanium Porous Structures: A Critical Review. *Biomimetics* **2023**, *8*, 546. [CrossRef] [PubMed]
4. Vanaclocha, A.; Vanaclocha, V.; Atienza, C.M.; Jordá-Gómez, P.; Primo-Capella, V.; Blasco, J.R.; Portolés, L.; Saiz-Sapena, N.; Vanaclocha, L. Effect of Ti6Al4V Alloy Surface and Porosity on Bone Osseointegration: In Vivo Pilot Study in Rabbits. *Materials* **2025**, *18*, 2141. [CrossRef] [PubMed]
5. Gain, A.K.; Cui, Y.; Zhang, L. Pore-Gradient Ti6Al4V Alloy Mimicking the Properties of Human Cortical Bones: The Design of TPMS Structures by Selective Laser Melting. *Mater. Sci. Eng. A* **2024**, *915*, 147220. [CrossRef]
6. Paul, A.R.; Singh, S.; Hirwani, J.; Yadav, S.; Dekiwadia, C.; Mukherjee, M.; Kalyanasundaram, D. Effect of Heat Treatment on the Material Property and Cell Viability of Wire Arc Additively Manufactured Ti6Al4 V. *ACS Appl. Bio Mater.* **2024**, *7*, 3096–3109. [CrossRef] [PubMed]

7. Das, B.; Sahoo, N.; Patel, P.; Ghosh, A.; Khan, M.A.; Bhushan, B.; Madan, R.; Shrivastava, P.; Msomi, V. Wire Arc Additive Manufacturing (WAAM): A Comprehensive Review of Process, Materials, Modelling, Artificial Intelligence, and Industrial Applications. *J. Alloys Compd.* **2026**, *1058*, 186347. [CrossRef]
8. Kiselevskiy, M.V.; Anisimova, N.Y.; Novruzov, K.M.; Kapustin, A.V.; Ryzhkin, A.A.; Abramova, M.M.; Enikeev, N.A. Topology-Defined Bioactive Properties of Porous Ti-6Al-4V Scaffolds Produced by Laser Powder Bed Fusion. *Mater. Lett.* **2024**, *377*, 137528. [CrossRef]
9. Aversa, A.; Carrozza, A.; Mercurio, V.; Calignano, F.; Sereda, O.; Pejchal, V.; Lombardi, M. A Comparison Between the Residual Stresses of Ti6Al4V and Ti-6Al-2Sn-4Zr-6Mo Processed by Laser Powder Bed Fusion. *Materials* **2025**, *18*, 689. [CrossRef] [PubMed]
10. Zarei, M.A.; Shabestari, M.G.; Shabestari, S.G.; Abedi, H. Microstructural Heterogeneity and Anisotropic Mechanical Properties of Titanium Alloys Manufactured by Wire Arc Additive Manufacturing: A Review. *J. Mater. Res. Technol.* **2025**, *36*, 8381–8409. [CrossRef]
11. Lakroune, Y.; Connétable, D.; Hugues, J.; Hermantier, P.; Barriobero-Vila, P.; Dehmas, M. Microstructural Evolution during Post Heat Treatment of the Ti–6Al–4V Alloy Manufactured by Laser Powder Bed Fusion. *J. Mater. Res. Technol.* **2023**, *23*, 1980–1994. [CrossRef]
12. Su, C.; Yu, H.; Wang, Z.; Yang, J.; Zeng, X. Controlling the Tensile and Fatigue Properties of Selective Laser Melted Ti–6Al–4V Alloy by Post Treatment. *J. Alloys Compd.* **2021**, *857*, 157552. [CrossRef]
13. Lin, J.J.; Lv, Y.H.; Liu, Y.X.; Xu, B.S.; Sun, Z.; Li, Z.G.; Wu, Y.X. Microstructural Evolution and Mechanical Properties of Ti-6Al-4V Wall Deposited by Pulsed Plasma Arc Additive Manufacturing. *Mater. Des.* **2016**, *102*, 30–40. [CrossRef]
14. Ty, A.; Balcaen, Y.; Mokhtari, M.; Alexis, J. Influence of Deposit and Process Parameters on Microstructure and Mechanical Properties of Ti6Al4V Obtained by DED-W (PAW). *J. Mater. Res. Technol.* **2022**, *18*, 2853–2869. [CrossRef]
15. Zhang, J.; Zhou, S.; Li, X.; Yin, J.; Zhou, S.; Guo, X.; Yang, G. Effect of Interlayer-Compressed Argon Gas Active Cooling on Microstructure and Properties of Ti–6Al–4V Fabricated by WAAM. *Adv. Eng. Mater.* **2023**, *25*, 2300618. [CrossRef]
16. Nguyen, H.D.; Pramanik, A.; Basak, A.K.; Dong, Y.; Prakash, C.; Debnath, S.; Shankar, S.; Jawahir, I.S.; Dixit, S.; Buddhi, D. A Critical Review on Additive Manufacturing of Ti-6Al-4V Alloy: Microstructure and Mechanical Properties. *J. Mater. Res. Technol.* **2022**, *18*, 4641–4661. [CrossRef]
17. Liu, S.; Shin, Y.C. Additive Manufacturing of Ti6Al4V Alloy: A Review. *Mater. Des.* **2019**, *164*, 107552. [CrossRef]
18. Bermingham, M.J.; Nicastro, L.; Kent, D.; Chen, Y.; Dargusch, M.S. Optimising the Mechanical Properties of Ti-6Al-4V Components Produced by Wire + Arc Additive Manufacturing with Post-Process Heat Treatments. *J. Alloys Compd.* **2018**, *753*, 247–255. [CrossRef]
19. Chen, Z.; Peng, Y.; Zhang, X.; Fan, J.; He, S.; Kong, J.; Wang, K. Influence of Trace Silicon Addition on Microstructure and Properties of Ti6Al4V Fabricated by Wire Arc Additive Manufacturing. *J. Mater. Res. Technol.* **2023**, *23*, 1347–1359. [CrossRef]
20. Xiaolong, C.; Zulei, L.; Yanhua, G.; Zhonggang, S.; Yaoqi, W.; Lian, Z. A Study on the Grain Refinement Mechanism of Ti-6Al-4V Alloy Produced by Wire Arc Additive Manufacturing Using Hydrogenation Treatment Processes. *J. Alloys Compd.* **2022**, *890*, 161634. [CrossRef]
21. Sun, Z.; Qi, F.; Guo, Y.; Wang, Y.; Chang, H.; Wu, F.; Chen, W.; Ji, X. The Effect of Hydrogen on the Grain Refinement and Mechanisms for Ti6Al4V Alloys during Laser Melting Deposition. *J. Alloys Compd.* **2021**, *877*, 160122. [CrossRef]
22. Syed, A.K.; Zhang, X.; Caballero, A.; Shamir, M.; Williams, S. Influence of Deposition Strategies on Tensile and Fatigue Properties in a Wire + Arc Additive Manufactured Ti-6Al-4V. *Int. J. Fatigue* **2021**, *149*, 106268. [CrossRef]
23. Siddiqui, N.A.; Muzamil, M.; Jamil, T.; Hussain, G. Heat Sources in Wire Arc Additive Manufacturing and Their Impact on Macro-Microstructural Characteristics and Mechanical Properties—An Overview. *Smart Mater. Manuf.* **2025**, *3*, 100059. [CrossRef]
24. Zhang, T.; Liu, C.-T. Design of Titanium Alloys by Additive Manufacturing: A Critical Review. *Adv. Powder Mater.* **2022**, *1*, 100014. [CrossRef]
25. Su, J.; Jiang, F.; Li, J.; Tan, C.; Xu, Z.; Xie, H.; Liu, J.; Tang, J.; Fu, D.; Zhang, H.; et al. Phase Transformation Mechanisms, Microstructural Characteristics and Mechanical Performances of an Additively Manufactured Ti-6Al-4V Alloy under Dual-Stage Heat Treatment. *Mater. Des.* **2022**, *223*, 111240. [CrossRef]
26. Wang, M.; Yan, H.; Lu, Q.; Zhang, P.; Liu, K. Selective Laser Melted Ti-6Al-4V Alloy after Post-Heat Treatments: Microstructure, Mechanical Properties and Fatigue Behavior. *J. Mater. Eng. Perform.* **2025**, *34*, 5381–5393. [CrossRef]
27. Wang, J.; Lin, X.; Wang, M.; Li, J.; Wang, C.; Huang, W. Effects of Subtransus Heat Treatments on Microstructure Features and Mechanical Properties of Wire and Arc Additive Manufactured Ti–6Al–4V Alloy. *Mater. Sci. Eng. A* **2020**, *776*, 139020. [CrossRef]
28. Gatina, S.; Gareev, A.; Stotskiy, A.; Ryzhkin, A.; Polyakova, V.; Semenova, I.; Enikeev, N.A. Improving the Mechanical Performance of L-PBF Ti-6Al-4V Alloy by Thermal Cycling for Trimodal A+α' Structure Formation. *Mater. Sci. Eng. A* **2026**, *949*, 149472. [CrossRef]

29. Semenova, I.P.; Shchitsyn, Y.D.; Trushnikov, D.N.; Gareev, A.I.; Polyakov, A.V.; Pesin, M.V. Microstructural Features and Microhardness of the Ti-6Al-4V Alloy Synthesized by Additive Plasma Wire Deposition Welding. *Materials* **2023**, *16*, 941. [CrossRef] [PubMed]
30. *ISO 6892-1:2019*; Metallic Materials—Tensile Testing—Part 1: Method of Test at Room Temperature. International Organization for Standardization: Geneva, Switzerland, 2019.
31. Ter Haar, G.M.; Becker, T.H. Selective Laser Melting Produced Ti-6Al-4V: Post-Process Heat Treatments to Achieve Superior Tensile Properties. *Materials* **2018**, *11*, 146. [CrossRef] [PubMed]
32. Laskowska, D.; Bałasz, B.; Żurawski, Ł. Evolution of the Metallographic Structure of Additively Manufactured Ti-6Al-4V and Ti-6Al-7Nb Titanium Alloys. *Materials* **2026**, *19*, 80. [CrossRef] [PubMed]
33. Pasang, T.; Tavlovich, B.; Yannay, O.; Jackson, B.; Fry, M.; Tao, Y.; Turangi, C.; Wang, J.-C.; Jiang, C.-P.; Sato, Y.; et al. Directionally-Dependent Mechanical Properties of Ti6Al4V Manufactured by Electron Beam Melting (EBM) and Selective Laser Melting (SLM). *Materials* **2021**, *14*, 3603. [CrossRef] [PubMed]
34. El-Hadad, S.; Nady, M.; Khalifa, W.; Shash, A. Influence of Heat Treatment Conditions on the Mechanical Properties of Ti–6Al–4V Alloy. *Can. Metall. Q.* **2018**, *57*, 186–193. [CrossRef]
35. Elshaer, R.N.; El-Hadad, S.; Nofal, A. Influence of Heat Treatment Processes on Microstructure Evolution, Tensile and Tribological Properties of Ti6Al4V Alloy. *Sci. Rep.* **2023**, *13*, 11292. [CrossRef] [PubMed]
36. Yamanaka, K.; Kuroda, A.; Ito, M.; Mori, M.; Bian, H.; Shobu, T.; Sato, S.; Chiba, A. Quantifying the Dislocation Structures of Additively Manufactured Ti–6Al–4V Alloys Using X-Ray Diffraction Line Profile Analysis. *Addit. Manuf.* **2021**, *37*, 101678. [CrossRef]
37. Chen, J.; Fabijanic, D.; Zhang, T.; Lui, E.W.; Brandt, M.; Xu, W. Deciphering the Transformation Pathway in Laser Powder-Bed Fusion Additive Manufacturing of Ti-6Al-4V Alloy. *Addit. Manuf.* **2022**, *58*, 103041. [CrossRef]
38. Motyka, M. Martensite Formation and Decomposition during Traditional and AM Processing of Two-Phase Titanium Alloys—An Overview. *Metals* **2021**, *11*, 481. [CrossRef]
39. Arasappan, R.K.; Tariq, H.M.R.; Baek, H.-S.; Kim, M.; Jun, T.-S. Crystallographic Texture and Phase Transformation in Titanium Alloys Fabricated via Powder Bed Fusion Processes: A Comprehensive Review. *Metals* **2026**, *16*, 25. [CrossRef]
40. Saumitra, V.; Gonnabattula, A.; Kumar, V.A.; Kanjarla, A.K. On the Nature of Variant Selection along Build Direction in Additively Manufactured Ti–6Al–4V Walls. *Materialia* **2025**, *44*, 102523. [CrossRef]
41. Davis, A.E.; Donoghue, J.; Kennedy, J.R.; Byres, N.; Prangnell, P.B. In-Situ Observation of Single Variant α Colony Formation in Ti-6Al-4V. *Acta Mater.* **2021**, *220*, 117315. [CrossRef]
42. Mahmud, A.; Huynh, T.; Zhou, L.; Hyer, H.; Mehta, A.; Imholte, D.D.; Woolstenhulme, N.E.; Wachs, D.M.; Sohn, Y. Mechanical Behavior Assessment of Ti-6Al-4V ELI Alloy Produced by Laser Powder Bed Fusion. *Metals* **2021**, *11*, 1671. [CrossRef]
43. Zykova, A.; Panfilov, A.; Vorontsov, A.; Shmakov, V.; Savchenko, N.; Gurianov, D.; Gusarenko, A.; Utyaganova, V.; Krasnoveikin, V.; Tarasov, S. Microstructural and Phase Evolution of Ti6Al4V in Electron Beam Wire Additive Manufacturing and on the Subtransus Quenching and Normalization. *Mater. Sci. Eng. A* **2024**, *898*, 146384. [CrossRef]
44. Collins, D.; Gussev, M.; Taller, S.; Byun, T.S.; Massey, C. Assessing the Viability of a New Subsize Tensile Specimen Geometry for Evaluation of Structural Nuclear and Additively Manufactured Materials. *J. Nucl. Mater.* **2025**, *612*, 155831. [CrossRef]

Disclaimer/Publisher's Note: The statements, opinions and data contained in all publications are solely those of the individual author(s) and contributor(s) and not of MDPI and/or the editor(s). MDPI and/or the editor(s) disclaim responsibility for any injury to people or property resulting from any ideas, methods, instructions or products referred to in the content.